# Electronic Supplementary Information: Tuning the chemical composition of binary alloy nanoparticles to prevent their dissolution

Luis A. Cipriano,*[a] Henrik H. Kristoffersen,[a] Renan Lopes Munhos,[b] Rebecca Pittkowski,[a] Matthias Arenz*[a,b] and Jan Rossmeisl[a]

[a]Department of Chemistry, Center for High Entropy Alloy Catalysis, University of Copenhagen, 2100 Copenhagen, Denmark

[b]Department for Chemistry, Biochemistry and Pharmaceutical Sciences, University of Bern, 3012 Bern, Switzerland

**Section S1.** Equations to calculate the dissolution percentage and the percentage of A atoms at the surface of the nanoparticles post-dissolution process (Pd atoms at the surface).

For each nanoparticle, nine molar fractions of protective material have been considered and 500 random structures were generated for each molar fraction, with a total of 4500 structures per nanoparticle.

$$Dissolution\ \% = 100 - \left( \frac{\frac{1}{500}\sum_{i=1}^{500} X_i}{N_{Atoms}} \times 100 \right)$$

Where $X_i$ corresponds to the number of remaining atoms in the nanoparticle and $N_{Atoms}$ to the number of atoms in the nanoparticle previous dissolution.

$$Pd\ at\ the\ surface\ \% = \frac{\frac{1}{500}\sum_{i=1}^{500} A^{Surf}_{i}}{\frac{1}{500}\sum_{i=1}^{500} A^{Surf}_{i} + B^{Surf}_{i}} \times 100$$

Where $A^{Surf}_{i}$ corresponds to the number of Pd atoms at the surface of the nanoparticle (exposed atoms with coordination number ≤ 11) and $A^{Surf}_{i} + B^{Surf}_{i}$ to the total number of atoms at the surface of the nanoparticle (Pd and Au atoms).

**Section S2.** Modeling nanoparticles with three exposed facets: (100), (110), and (111)

To assess the effect of the number of exposed crystallographic facets on the dissolution process, we have considered the following nanoparticles: a) 2.20nm, b) 2.48nm, c) 3.17nm, and d) 4.14nm. The shape of each NP is shown in Fig. S1.

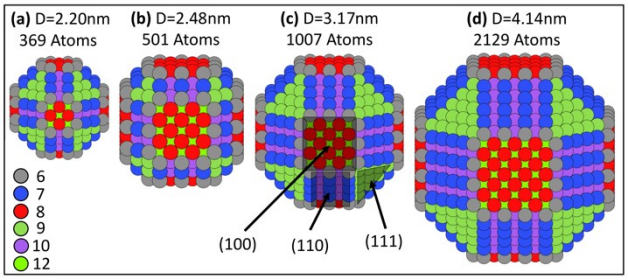


***Fig. S1*** *Nanoparticles with three exposed facets: (100), (110), and (111). Color coding in the nanoparticles shows the number of neighboring atoms that each atom has. Red, blue, and green balls also represent the (100), (110), and (111) facets.*

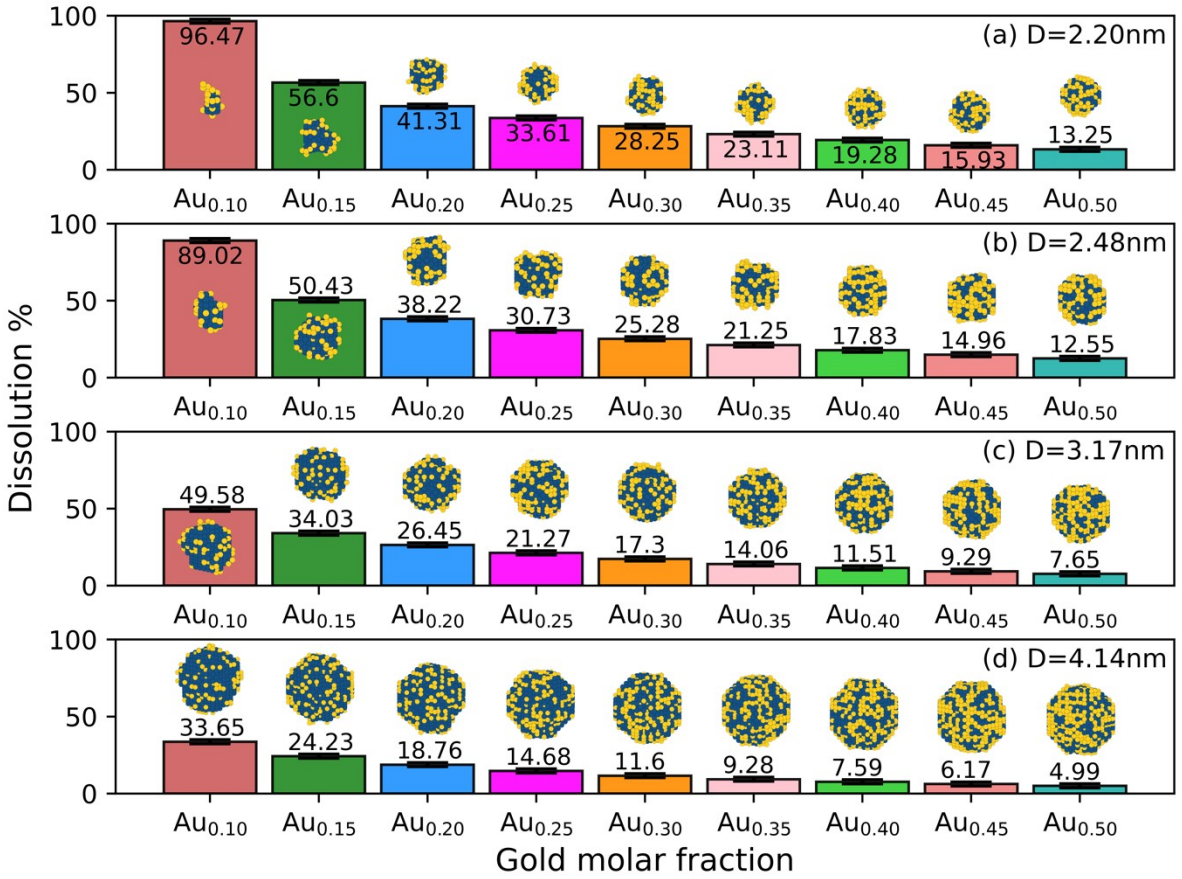


***Fig. S2*** *Mean values of the dissolution percentage on nanoparticles as a function of the gold molar fraction. (a) NPs of 2.20nm, (b) NPs of 2.48 nm, (c) NPs of 3.17nm, and (d) NPs of 4.14nm. The dark blue and yellow balls represent the palladium and gold atoms, respectively.*

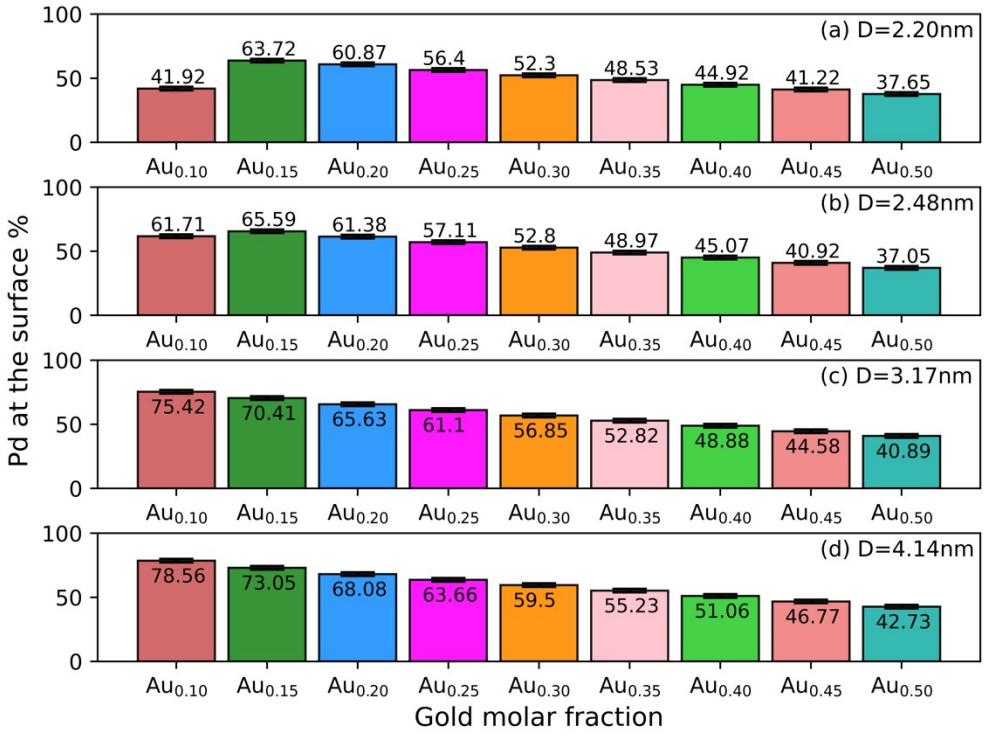


***Fig. S3*** *Mean values of the percentage of Pd atoms at the surface of the nanoparticles post-dissolution process as a function of the gold molar fractions. (a) NPs of 2.20nm, (b) NPs of 2.48nm, (c) NPs of 3.17nm, and (d) NPs of 4.14nm.*

**Section S3.** Standard electrode potential at 298.15 K (25°C) and 0.1 MPa (1 bar) – 1M HCl

The standard electrode potentials vs SHE for Au and Pd ions under HCl electrolyte have been calculated through the standard Gibbs free energy of formation ($G_f°$) as follows:

$$E^{\circ} = \frac{\sum \Delta G^{\circ}_{left} - \sum \Delta G^{\circ}_{right}}{nF}$$

***Table S1*** *Standard electrode potentials vs SHE for Au and Pd ions under HCl electrolyte, the standard Gibbs free energy of formation ($G_f°$) were taken from the NBS tables of chemical thermodynamic properties: Selected values for inorganic and C and C2 organic substances in SI units.*[1]

| Element | Half-reaction | | | | | $E°$ / V vs SHE |
|---|---|---|---|---|---|---|
| Cl | $Cl_2(g)$ | + $2e^-$ | ⇌ | $2Cl^-$ | | 1.36 |
| $\Delta G_f°$ (kJ/mol) | 0 | 0 | | -131.23 | | |
| Au | Au(s) | + $4Cl^-$ | ⇌ | $AuCl_4^-$ | + $3e^-$ | 1.00 |
| $\Delta G_f°$ (kJ/mol) | 0 | 4*-131.23 | | -235.14 | 0 | |
| | | | | | | |
| Pd | Pd(s) | + $4Cl^-$ | ⇌ | $PdCl_4^{2-}$ | + $2e^-$ | 0.56 |
| $\Delta G_f°$ (kJ/mol) | 0 | 4*-131.23 | | -417.10 | 0 | |

**Section S4.** Surface cohesive energy of kink atoms in pure metal surfaces

As mentioned in the main text, kink atoms are special atoms because their remotion leaves the same surface behind, Fig S4 shows the side and top view of a kink surface.

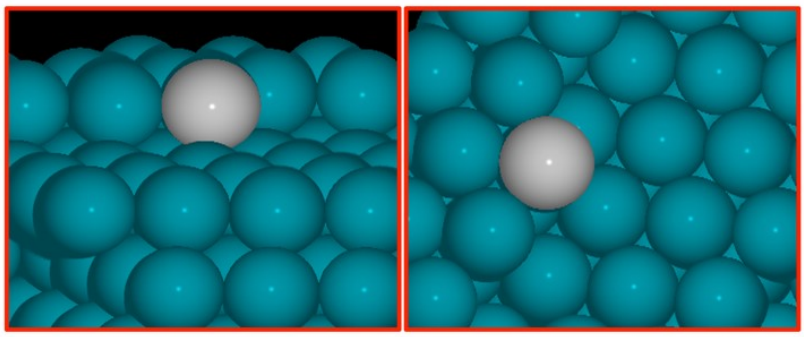

***Fig. S4*** *Side and top view of the kink surface. The gray ball highlights the kink atom.*

The surface cohesive energy for the remotion of kink atoms from the kink surfaces was calculated as follows and the results are reported in Table S2:

$$E_{kink} = E_{M}^{kink} - E_{M}^{not-kink}$$

Where $E_M^{kink}$ is the kink surface energy for each metal and $E_M^{not\text{-}kink}$ is the energy of the same kink surface without the kink atom (M = Au or Pd).

***Table S2*** *Optimized bulk lattice parameter for each metal (a, in Å) and its corresponding energy ($E_{bulk}$, in eV), and the energy of removing a kink atom from the kink surface ($E_{kink}$, in eV).*

| M | *a* | $E_{Bulk}$ | $E_{Kink}$ |
|---|---|---|---|
| Au | 4.2097 | -2.56 | -2.58 |
| Pd | 3.9627 | -3.22 | -3.22 |

**Section S5.** Initial cyclic voltammetry of pure Pd, $Au_{0.20}Pd_{0.80}$, and $Au_{0.40}Pd_{0.60}$ nanoparticles immobilized on a GC disk RDE.

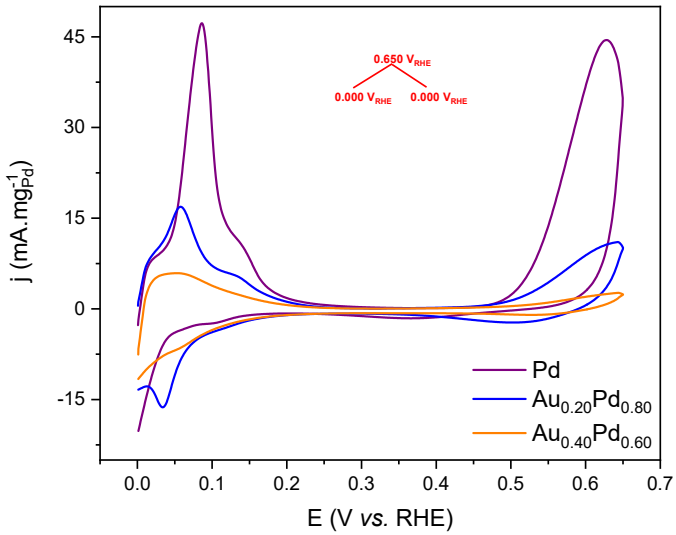


***Fig. S5*** *Initial cyclic voltammograms of pure Pd, $Au_{0.20}Pd_{0.80}$, and $Au_{0.40}Pd_{0.60}$ nanoparticles immobilized on a GC disk of an RDE. The CVs were recorded at room temperature with 5 mV $s^{-1}$ in 1 M HCl aqueous electrolyte. RHE and Glassy Carbon electrodes were used as reference and counter electrodes, respectively.*

**Section S6.** Scanning Electron Microscopy (SEM) coupled to Energy Dispersive X-Ray (EDX) analysis of Pd, $Au_{0.20}Pd_{0.80}$, and $Au_{0.40}Pd_{0.60}$ nanoparticles.

For the SEM-EDX analysis, a layer of nanoparticles was deposited onto a graphite surface glued with double-sided carbon tape on a stainless-steel holder. The analyses were performed with a Zeiss Gemini 450 SEM equipped with a X-max 150 EDX detector by Oxford Instruments.

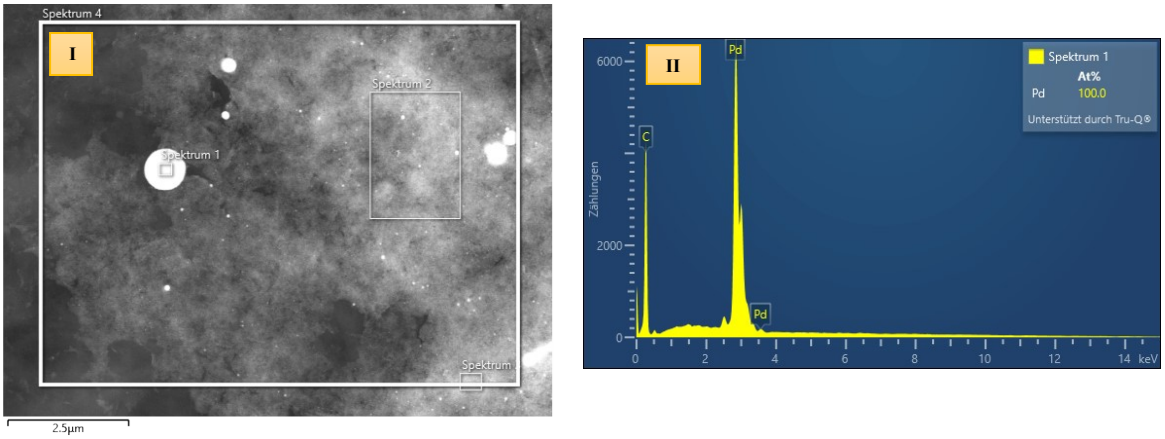

***Fig. S6a I.*** *Representative SEM image of Pd nanoparticles acquired at 20kV, 200 pA, 10,000x magnification with Back Scattering Detector.* ***II.*** *Representative EDX spectrum taken at the point named "Spektrum 1", where particle agglomeration was observed.*

11 spectra were acquired at 10k x, 20k x, and 50k x magnification. All quantified 100% Palladium.

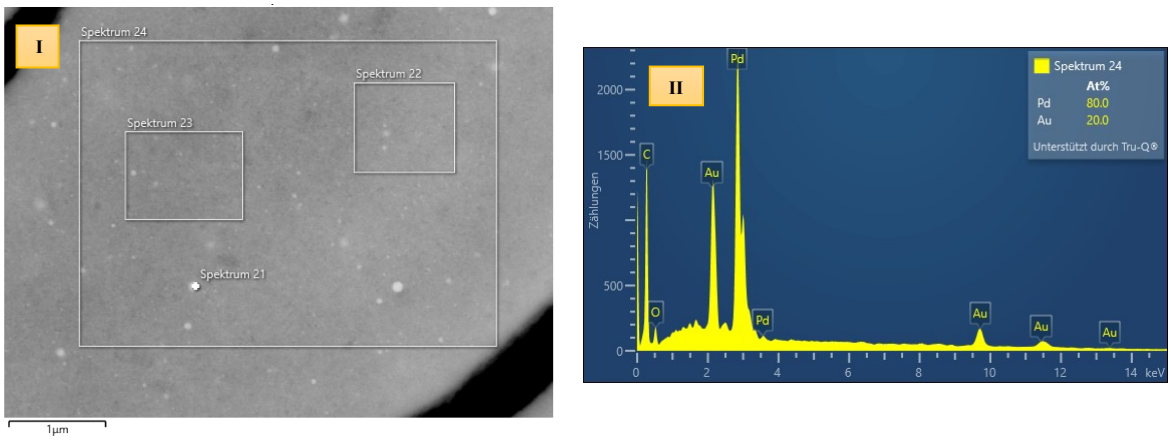


***Fig. S6b I****. Representative SEM image of $Au_{20}Pd_{80}$ nanoparticles acquired at 20kV, 200 pA, 20,000x magnification with Back Scattering Detector.* ***II****. Representative EDX spectrum taken at the point named "Spektrum 24". The determined atomic percentage (At %) of $Au_{20}Pd_{80}$ was 80% Pd and 20% Au.*

14 spectra were measured at 10k x, 20k x, and 50k x magnification. The results are shown in **Table S3b1** and summarized as the minimum, maximum, average, and standard deviation in **Table S3b2**.

***Table S3b1*** *EDX quantification of the atomic composition of $Au_{20}Pd_{80}$ nanoparticles.*

| Name of the Spectrum | Pd (%) | Au (%) | Sum (%) |
|---|---|---|---|
| Spektrum 12 | 80.69 | 19.31 | 100.00 |
| Spektrum 15 | 80.98 | 19.02 | 100.00 |
| Spektrum 17 | 80.72 | 19.28 | 100.00 |
| Spektrum 18 | 80.41 | 19.59 | 100.00 |
| Spektrum 19 | 80.32 | 19.68 | 100.00 |
| Spektrum 20 | 80.37 | 19.63 | 100.00 |
| Spektrum 21 | 80.47 | 19.53 | 100.00 |
| Spektrum 22 | 79.97 | 20.03 | 100.00 |
| Spektrum 23 | 80.28 | 19.72 | 100.00 |
| Spektrum 24 | 79.97 | 20.03 | 100.00 |
| Spektrum 25 | 80.56 | 19.44 | 100.00 |
| Spektrum 26 | 80.55 | 19.45 | 100.00 |
| Spektrum 27 | 80.42 | 19.58 | 100.00 |
| Spektrum 28 | 80.09 | 19.91 | 100.00 |

***Table S3b2*** *Summary of EDX quantification in* ***Table S6b1****.*

| Statistic | Pd (%) | Au (%) |
|---|---|---|
| Maximum | 80.98 | 20.03 |
| Minimum | 79.97 | 19.02 |
| **Average** | 80.41 | 19.59 |
| Standard deviation | 0.29 | 0.29 |

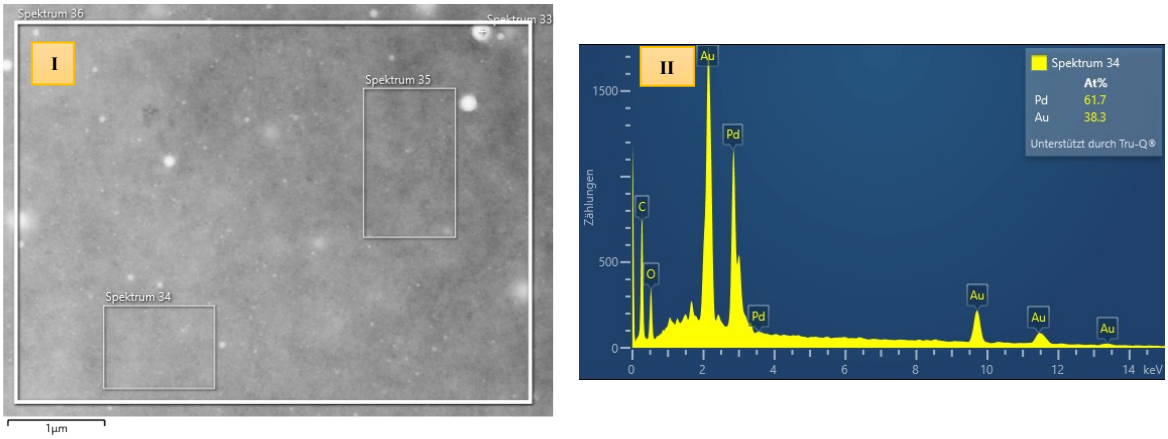


***Fig. S6c I.*** *Representative SEM image of* $Au_{40}Pd_{60}$ *nanoparticles acquired at 20kV, 200 pA, 20,000x magnification with Back Scattering Detector.* ***II.*** *Representative EDX spectrum taken at the point named "Spektrum 34". The determined atomic percentage (At%) of* $Au_{40}Pd_{60}$ *was 61.7% Pd and 38% Au.*

12 spectra were measured at 10k x, 20k x, and 50k x magnification. The results are shown in **Table S3c1** and summarized as minimum, maximum, average, and standard deviation, in **Table S3c2**.

***Table S3c1*** *EDX quantification of the atomic composition of* $Au_{40}Pd_{60}$ *nanoparticles.*

| Name of the Spectrum | Pd (%) | Au (%) | Summatory (%) |
|---|---|---|---|
| Spektrum 29 | 62.30 | 37.70 | 100.00 |
| Spektrum 30 | 63.34 | 36.66 | 100.00 |
| Spektrum 31 | 64.13 | 35.87 | 100.00 |
| Spektrum 32 | 63.45 | 36.55 | 100.00 |
| Spektrum 33 | 64.13 | 35.87 | 100.00 |
| Spektrum 34 | 61.69 | 38.31 | 100.00 |
| Spektrum 35 | 62.82 | 37.18 | 100.00 |
| Spektrum 36 | 63.08 | 36.92 | 100.00 |
| Spektrum 37 | 64.62 | 35.38 | 100.00 |
| Spektrum 38 | 63.66 | 36.34 | 100.00 |
| Spektrum 39 | 63.35 | 36.65 | 100.00 |
| Spektrum 40 | 64.40 | 35.60 | 100.00 |

***Table S3c2*** *Summary of EDX quantification in* ***Table S6c1****.*

| Statistic | Pd (%) | Au (%) |
|---|---|---|
| Maximum | 64.62 | 38.31 |
| Minimum | 61.69 | 35.38 |
| **Average** | 63.41 | 36.59 |
| Standard deviation | 0.86 | 0.86 |

**Section S7.** Inductively Coupled Plasma Mass Spectroscopy (ICP-MS) quantification was performed as described in the section Experimental Details and the results are shown in **Fig. S7**.

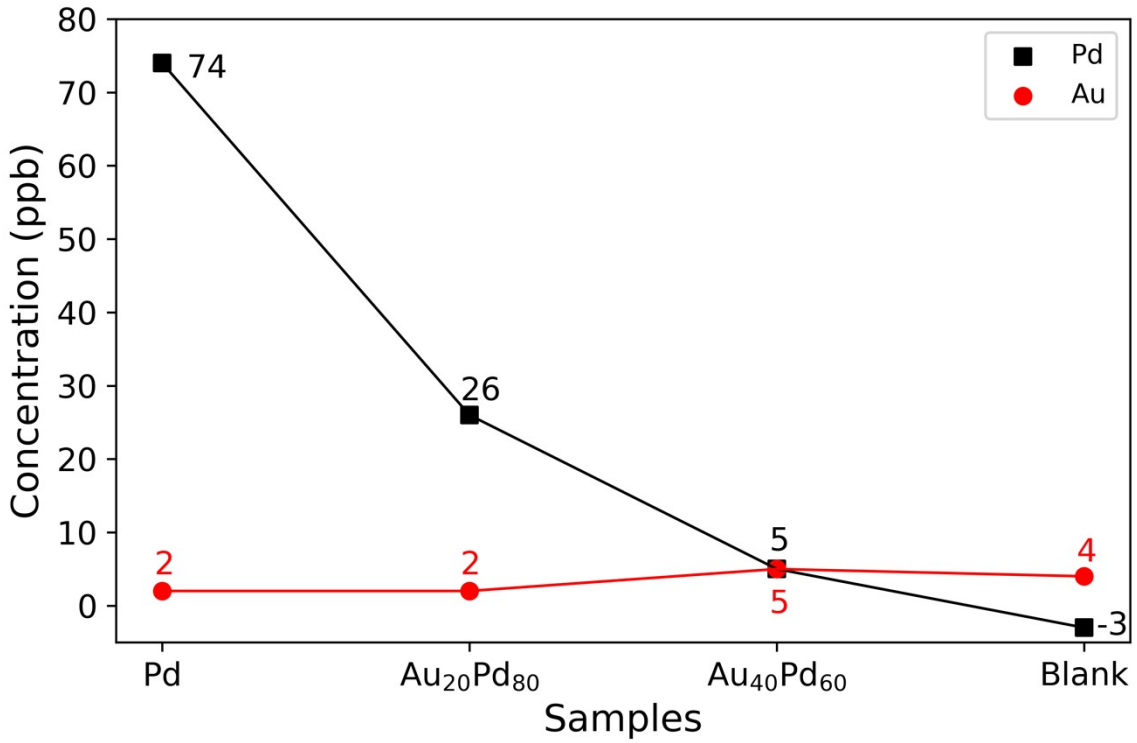


***Fig. S7** ICP-MS concentration of Au and Pd found in the electrolyte after triangular perturbation of the potential between 0.00$V_{RHE}$ and 0.650$V_{RHE}$ with 30 cycles. The concentrations are expressed in Parts Per Billion (ppb) which is equivalent to $\mu g.L^{-1}$.*

**Section S8.** The use of the $H_{UPD}$ charge to probe the active surface area is rationalized in **Fig. S8** below.

The CO-stripping measurement was performed with $Au_{0.20}Pd_{0.80}$ as catalyst in 0.1M $HClO_4$ (70% pure, Sigma-Aldrich) supporting electrolyte. From the calculated charges shown in **Fig. S8**, the CO (CarbaGas/Air Liquide, Switzerland) oxidation charge represents almost twice the $H_{UPD}$ charge. Considering that hydrogen oxidation is a one electron process, while two electrons are required to oxidize CO, CO stripping leads to the same active surface area as $H_{UPD}$ indicating a minor effect of the ligand effect on weakly adsorbing hydrogen (as compared

to the more strongly adsorbing CO molecule). The E *vs.* i transients were acquired between 0.1 $V_{RHE}$ and 1.3 $V_{RHE}$ at scan rate 20 mV $s^{-1}$.

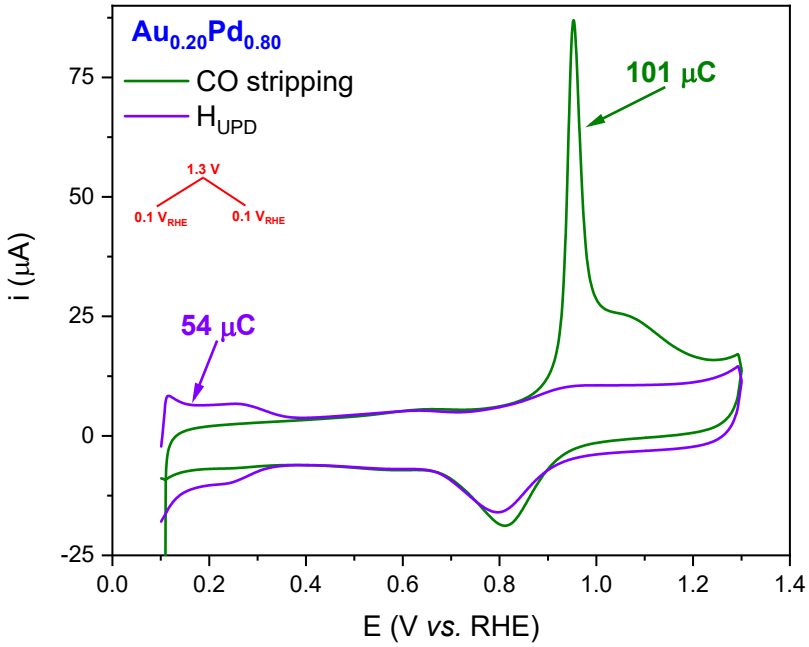


***Fig. S8*** *E* vs. *i transients acquired for* $Au_{0.20}Pd_{0.80}$ *catalyst in 0.1 M aqueous* $HClO_4$ *at room temperature and scan rate of 20* $mV\ s^{-1}$.

**Section S9.** Structural determination of Pd, $Au_{0.20}Pd_{0.80}$, and $Au_{0.40}Pd_{0.60}$ NPs by High Resolution Transmission Electron Microscopy (HR-TEM) and X-ray Diffraction (XRD).

The orientation of the exposed crystal faces was calculated from the FTT images shown below for each particle. The lattice parameter was calculated, and the faces were defined from the tables available in software XPert-Highscore version of 2008.

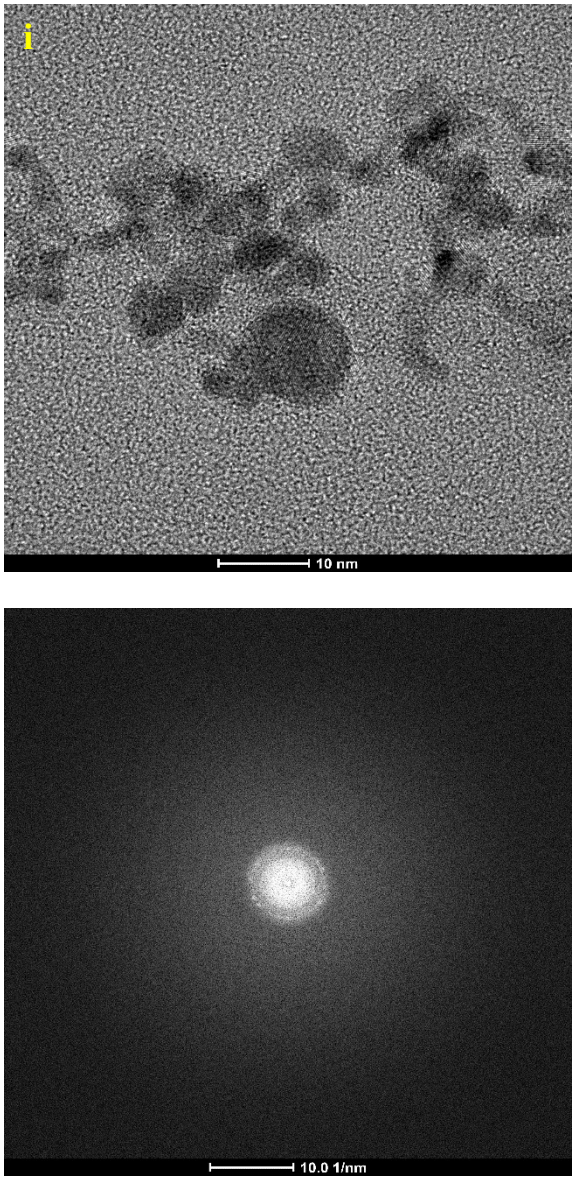


***Fig. S9a i.*** *HR-TEM micrograph of pure Pd NPs.* ***ii.*** *FTT of* ***i****, the exposed crystal orientations calculated from the FTT of* ***i*** *were Pd(111) and Pd(002).*

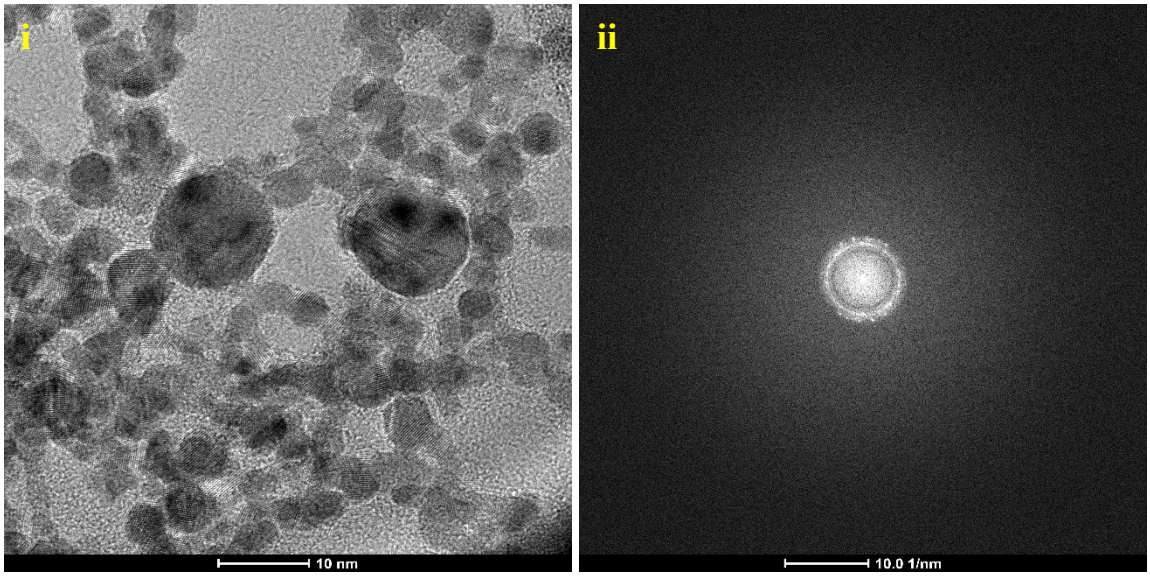


***Fig. S9b i.*** *HR-TEM micrograph of pure* $Au_{0.20}Pd_{0.80}$ *NPs.* ***ii.*** *FTT of* ***i****, the exposed crystal orientations calculated from the FFT of* ***i*** *were (111) and (002).*

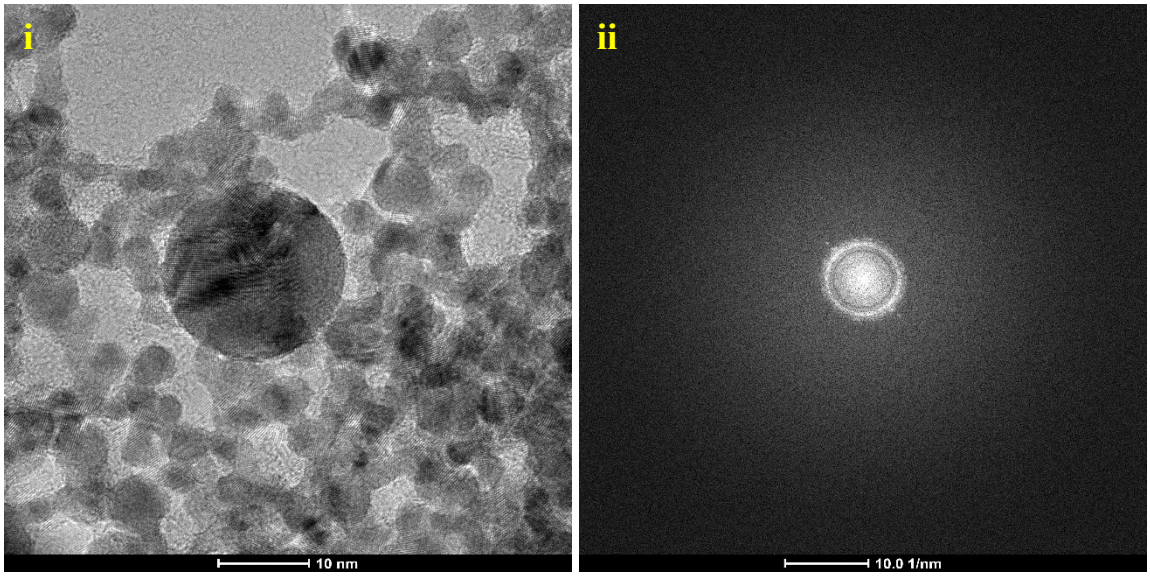


***Fig. S9c i.*** *HR-TEM micrograph of* $Au_{0.40}Pd_{0.60}$*NPs.* ***ii.*** *FTT of* ***i****, the exposed crystal orientations calculated from the FTT of* ***i*** *were (111), (002), and (022).*

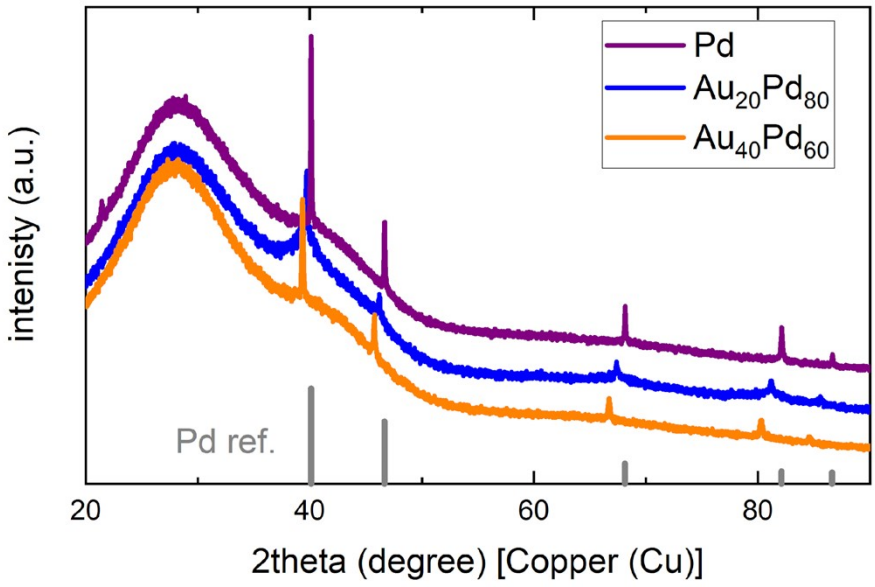


***Fig. S9d*** *Overview of the X-ray diffraction pattern collected for the different Pd-based particles, the diffraction patterns are plotted with a reference of bulk* fcc *Pd metal (lattice parameter a=3.89 Å). All Bragg peaks in the diffraction pattern of the experimental samples correspond to the ones expected for a* fcc *structure.*

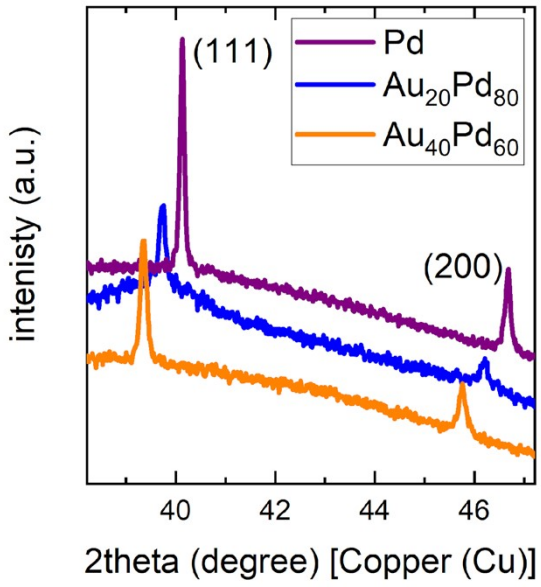


***Fig. S9e*** *Zoom on the (111) and (200) reflections of the collected X-ray diffraction patterns (Fig. S9d). The position of Bragg peaks and with that the lattice parameter shifts based on the respective Pd/Au ratio of the samples, agreeing with the single-phase solid solution behavior of the PdAu alloys.*

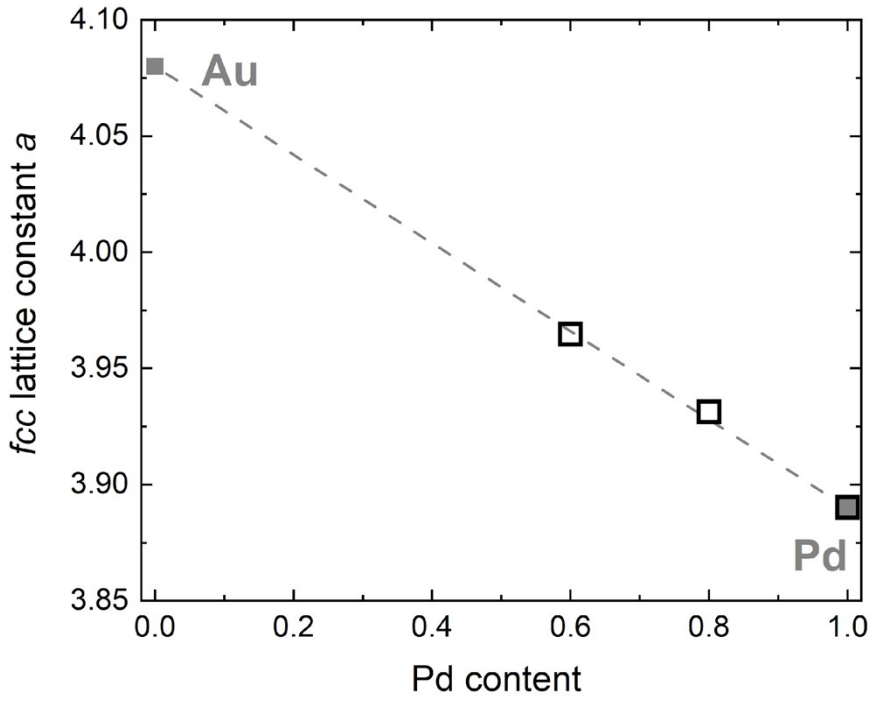


***Fig. S9f*** *Plot of the lattice parameters a, determined from the X-ray diffraction patterns of the three Pd-based samples, as a function of Pd content. The experimental lattice parameters a are well correlated with the expected lattice parameters which correspond to the nominal composition of PdAu alloys based on Vegard's law. The literature references for the* fcc *lattice parameters of Pd and Au are 3.89Å and 4.08 Å, respectively.*[2]

***Table S4.*** *Refined parameters obtained from Rietveld refinements by fitting an* fcc *model to the collected X-diffraction data*

| Sample | *a* (Å) | Size (µm) | Scale | Uiso (Å²) | wR (%) |
|---|---|---|---|---|---|
| **Pd** | 3.8901(1) | 1.15(3) | 0.9701 | 0.006(1) | 2.71 |
| **$Au_{0.20}Pd_{0.80}$** | 3.9309(9) | 0.05(3) | 0.9846 | 0.007(3) | 2.67 |
| **$Au_{0.40}Pd_{0.60}$** | 3.9646(2) | 0.10(8) | 0.9251 | 0.007(1) | 1.98 |

## References

1 D. D. Wagman, W. H. Evans, V. B. Parker, R. H. Schumm, I. Halow, S. M. Bailey, K. L. Churney and R. L. Nuttall, *J. Phys. Chem. Ref. Data*, 1982, **11**, 1–392.

2 Wyckoff R W G. “Cubic closest packed, ccp, structure “Crystal Structures 1 (1963) 7-83. *Second edition*. Interscience Publishers, New York, New York.